

# Optimizing Energy Efficiency of 5G RedCap Beam Management for Smart Agriculture Applications

Manishika Rawat, Matteo Pagin, *Student Member, IEEE*, Marco Giordani, *Member, IEEE*,  
Louis-Adrien Dufrene, Quentin Lampin, Michele Zorzi, *Fellow, IEEE*

**Abstract**—Beam management in 5G NR involves the transmission and reception of control signals such as Synchronization Signal Blocks (SSBs), crucial for tasks like initial access and/or channel estimation. However, this procedure consumes energy, which is particularly challenging to handle for battery-constrained nodes such as RedCap devices. Specifically, in this work we study a mid-market Internet of Things (IoT) Smart Agriculture (SmA) deployment where an Unmanned Autonomous Vehicle (UAV) acts as a base station “from the sky” (UAV-gNB) to monitor and control ground User Equipments (UEs) in the field. Then, we formalize a multi-variate optimization problem to determine the optimal beam management design for RedCap SmA devices in order to reduce the energy consumption at the UAV-gNB. Specifically, we jointly optimize the transmission power and the beamwidth at the UAV-gNB. Based on the analysis, we derive the so-called “regions of feasibility,” i.e., the upper limit(s) of the beam management parameters for which RedCap Quality of Service (QoS) and energy constraints are met. We study the impact of factors like the total transmission power at the gNB, the Signal-to-Noise Ratio (SNR) threshold for successful packet decoding, the number of UEs in the region, and the misdetection probability. Simulation results demonstrate that there exists an optimal configuration for beam management to promote energy efficiency, which depends on the speed of the UEs, the beamwidth, and other network parameters.

**Index Terms**—5G NR, 3GPP, beam management, energy consumption, optimization, smart agriculture.

## I. INTRODUCTION

As the world becomes increasingly interconnected, the 3rd Generation Partnership Project (3GPP) New Radio (NR) standard [2] for 5th generation (5G) networks represents a significant advancement in telecommunications, offering unprecedented high speed, reliability, and connectivity [3]. Specifically, 5G NR rests on three main service pillars, catering to specific requirements and applications [4]: (i) enhanced Mobile Broadband (eMBB), providing faster data speeds (up to 20 Gbps in ideal conditions) and greater capacity (up to 10

Mbit/s/m<sup>2</sup>) compared to previous generations, e.g., for high-definition video streaming or immersive AR/VR experience; (ii) Ultra-Reliable Low-Latency Communications (URLLC) supporting mission-critical applications (i.e., with around 1 ms round-trip delay) like autonomous vehicles or remote surgery; and (iii) massive Machine-Type Communications (mMTC), supporting interconnected networks of low-cost low-energy-consumption Internet of Things (IoT) sensors (with up to 10<sup>6</sup> connections per km<sup>2</sup>) that communicate and exchange data.

In particular, IoT applications span various sectors, from smart homes and cities to industrial automation (e.g., transportation and logistics) and healthcare (e.g., in smart hospitals and/or to facilitate automatic data collection and sensing) [5], [6]. Notably, the main requirements of IoT services are long transmission range (in the order of a few kilometers) and low energy consumption to support prolonged battery lifetime for sensors (up to 10 years). Along these lines, standardization bodies and industry players have contributed to develop various Low-Power Wide Area Network (LPWAN) technologies, such as Long Range (LoRa) [7], Narrowband-IoT (NB-IoT) [8], and SigFox [9], to provide a good balance between range and energy consumption [10] for low-cost low-complexity IoT use cases. However, the data rate of LPWAN systems is generally limited to a few hundreds of Kbps, which may not be compatible with the requirements of future IoT use cases, for example Indoor Factory (InF) and/or Smart Agriculture (SmA) applications. SmA, in particular, involves the use of IoT devices such as sensors, drones, and robots, to generate and distribute data to monitor, manage, and automate various agricultural processes (e.g., crop data collection and/or livestock monitoring) [11]. In this case, data rate requirements can be up to 100 Mbps [12] (e.g., when data is sent to optimize/assist farmers’ decisions), and the latency can be in the order of a few ms.

In this context, the 3GPP is actively promoting a new standard called Reduced Capability (RedCap) [13] to accommodate high-end IoT devices [14]. Specifically, RedCap is positioned to satisfy higher data rate and reliability, and lower latency than current LPWAN technologies, while promoting lower cost and complexity, longer battery life, and wider coverage than full-blown 5G NR solutions [2].

As in 5G NR, RedCap devices may operate in both Frequency Range 1 (between 410 and 7125 MHz) and Frequency Range 2 (between 24.25 and 52.6 GHz), i.e., in the lower part of the millimeter wave (mmWave) spectrum, to improve network performance [15]. However, mmWaves come with strict limitations in terms of propagation (mainly severe path loss and absorption), which requires the endpoints to communicate

Manishika Rawat was with the Department of Information Engineering (DEI) of the University of Padova, Italy. She is now with the Department of Electronics and Communication Engineering, IIT Roorkee, India. Email: manishika.rawat8@gmail.com

Matteo Pagin, Marco Giordani, and Michele Zorzi are with the Department of Information Engineering (DEI) of the University of Padova, Italy. Email: {paginmatte,giordani,zorzi}@dei.unipd.it.

Louis-Adrien Dufrene and Quentin Lampin are with Orange Labs, France. Email: {louisadrien.dufrene,quentin.lampin}@orange.com.

A preliminary version of this work was presented at the IEEE Global Communications Conference 2023 [1].

This work was partially supported by the European Union under the Italian National Recovery and Resilience Plan (NRRP) of NextGenerationEU, partnership on “Telecommunications of the Future” (PE0000001 - program “RESTART”).



Fig. 1. UE mobility model (left) and SMA scenario (right). During beam management,  $UE_k$  accumulates an angular offset  $\theta_k$  due to initial misalignment ( $\theta_{i,k}$ ) and mobility ( $\theta_{v,k}$ ).

through highly-directional transmissions via Multiple Input Multiple Output (MIMO) antenna arrays and beamforming. As such, the transmitter and the receiver need to establish and maintain precise beam alignment for communication, which may increase the control overhead. Along these lines, most prior works study algorithms that periodically align the transmitting and receiving beams to optimize the link quality [16]–[19]. For instance, Hussain *et al.* [17] proposed a dual-timescale learning-based algorithm to optimize the spectral efficiency by predicting beam dynamics and thus reducing the control overhead. Similarly, Scalabrin *et al.* [18] proposed an adaptive scheme to reduce the beam training overhead by controlling the beamwidth.

In 5G NR, beam alignment is determined and preserved by a control procedure referred to as beam management [20]. In this process, the Next Generation Node Base (gNB) continuously sends control signals at predefined intervals and directions in the form of Synchronization Signal Blocks (SSBs), possibly grouped into bursts. Upon receiving and detecting the SSBs, end users can identify the strongest beam to connect to, and the resulting direction of transmission towards the gNB. However, beam management consumes significant energy for sending and receiving control signals, especially when using narrow beams and short SSB periodicity [21]. While this might not be a critical concern for 5G NR systems, it may be challenging for low-complexity battery-powered RedCap devices, thus potentially degrading network performance. To date, only a few works explored the complexity and power consumption of 5G NR beam management for IoT (though not specifically for RedCap). For example, Zhao *et al.* [22] designed an efficient beam training scheme for IoT devices, although the evaluation is only in terms of the system capacity. Zeulin *et al.* [23] used a digital twin of an industrial IoT environment to predict beam dynamics and thus simplify the beam scanning procedure. Mukherjee *et al.* [24] studied the energy consumption of beam management in the context of spectrum sharing.

Recent efforts in the scientific community have explored several ways to simplify the 5G NR standard to optimize power consumption for RedCap devices [15]. These include, for example: (i) a simpler MIMO design at the user terminals, with much smaller form factor and fewer layers; (ii) the use of low-cost hardware components; (iii) the use of a lower

bandwidth compared to 5G NR, ranging from 50 to 100 MHz; (iv) relaxation of the maximum modulation order, from 6 to 4; and (v) the introduction of power saving functionalities, such as Extended Discontinuous Reception (eDRX) or wake-up signals. However, to the best of our knowledge, there has been little research specifically focusing on how to optimize control network procedures for RedCap, including beam management.

In our previous work [1], we addressed this issue in an InF scenario. Specifically, we described an algorithm to minimize the energy consumption during beam management by optimizing the number of antennas at the gNB, with constraints related to the maximum transmission power at the gNB and the probability of misdetection for the user terminals. However, we did not optimize the transmission power at the gNB. In fact, while for an InF scenario the gNB is generally connected to the electric grid and may not be power limited, there are some other scenarios where instead power is a critical parameter. Consider, for example, an SMA use case, as represented in Fig. 1, in which a Unmanned Autonomous Vehicle (UAV) acts as a gNB “from the sky” to collect data from sensors in the field, like in vineyards (e.g., one sensor per vine) or plantations (e.g., one sensor per fruit tree)<sup>1</sup>.

Now, UAVs use the battery for propulsion and hovering [26], so it becomes particularly important to minimize the energy consumption under several aspects, including at the control plane for network operations such as beam management.

To bridge these research gaps, in our paper we extend our previous work in [1] by optimizing the energy consumption of beam management for RedCap devices in an SMA scenario. Our contributions can be summarized as follows:

- We formalize a multi-variate optimization problem to minimize the energy consumption of RedCap beam management. We consider an aerial gNB onboard a UAV monitoring soil and/or supporting harvesting or pest monitoring of live stocks. Then, we jointly optimize the number of antennas (therefore the beamwidth) and the transmission power at the UAV-gNB. We set constraints in terms of the maximum transmission power that can

<sup>1</sup>Although most RedCap energy and/or complexity reduction techniques concern UE-side procedures, the RedCap framework is typically considered as an additional 5G use case targeting “devices” rather than UEs only [25]. Therefore, simplifications at the gNB are also included here.

- be used at the UAV-gNB to sustain the flight, and the misdetection probability for the ground terminals/sensors.
- As our optimization problem is non-convex, we propose to solve it via a Monte Carlo (MC) algorithm. In particular, we find the lower bound of the expression of the energy consumption of beam management, and show that its derivative is non-negative, so that our optimization problem chooses the minimum values of the optimization variables that meet the problem's constraints.
  - We run a vast simulation campaign to dimension beam management for RedCap devices in an SmA scenario. Numerical results are given as a function of many parameters, including the speed of the ground terminals, the number of SSBs per burst and the burst periodicity, the maximum transmission power at the UAV-gNB, and the number of ground terminals. We demonstrate that there exists an optimal configuration for beam management that can minimize the energy consumption at the UAV-gNB.
  - We derive the so-called "regions of feasibility," i.e., the upper limits of the beam management parameters, such as the number of SSBs per burst and the burst periodicity, where Quality of Service (QoS) constraints are met, e.g., in terms of misdetection probability. Based on that, we provide guidelines on the optimal beam management design for RedCap devices in an SmA scenario.

The rest of the paper is organized as follows. In Sec. II we present our system model (deployment, energy, mobility, and beam management). In Sec. III we describe our optimization problem, the impact of the number of antenna elements at the gNB and the transmission power on the QoS constraints, and provide some analytical results. In Sec. V we present the simulation results and provide design guidelines towards the optimal set of parameters for beam management. Finally, conclusions are given in Sec. VI.

## II. SYSTEM MODEL

In this section we present our deployment (Sec. II-A), beam management (Sec. II-B), energy consumption (Sec. II-C), and beam dynamics (Sec. II-D) models.

### A. Deployment Model

We consider a 3GPP Rural Macro (RMA) scenario [27] with a radius  $R$ , served by a UAV acting as a gNB and deployed at height  $h_{\text{gNB}}$ . The  $K$  RedCap User Equipments (UEs) of height  $h_{\text{UE}}$  are distributed uniformly in the serving region. The location of  $\text{UE}_k$ , for  $k \in \{1, 2, \dots, K\}$ , is given by the polar coordinates  $(d_k, \phi_k)$ , where  $d_k$  is the 2D distance between  $\text{UE}_k$  and the gNB, and  $\phi_k$  is the angle of  $\text{UE}_k$  with respect to the positive x-axis, measured counterclockwise. The UEs are assumed to be moving on a circle at constant velocity  $v$  in a counterclockwise direction.<sup>2</sup>

<sup>2</sup>Notice that the mobility model is defined only in terms of the tangential velocity  $v$ . However, in this paper we focus on the probability that a UE moves outside of the coverage of a certain beam, which indeed only depends on  $\phi_k$  and so on the tangential velocity. In fact, the normal component of the velocity has an impact only on  $d_k$ , and is thus neglected in this work.

If  $P_T$  is the transmission power at the gNB, then the average Signal-to-Noise Ratio (SNR) at  $\text{UE}_k$  can be expressed as  $P_T \gamma_k$ . In turn,  $\gamma_k$  can be defined as [28]

$$\gamma_k(d_{3D}) = \frac{\mathcal{H}_L P_T(d_{3D}) + \mathcal{H}_N(1 - P_r(d_{3D}))}{N_0 \cdot B / G_{\text{gNB},k} G_{\text{UE}}}, \quad (1)$$

where  $d_{3D} = \sqrt{(h_{\text{gNB}} - h_{\text{UE}})^2 + d_k^2}$  is the distance between the gNB and  $\text{UE}_k$ ,  $N_0$  is the noise Power Spectral Density (PSD) and  $B$  is the channel bandwidth.  $P_r(d_{3D})$  is the Line-of-Sight (LoS) probability, as described in [27], and  $\mathcal{H}_j$  represents the joint effect of path loss, shadowing and fading and is thus defined as

$$\mathcal{H}_j = |\mathfrak{h}_j^k|^2 / \text{PL}_j^k, \quad j \in \{\text{L}, \text{N}\}, \quad (2)$$

where  $\mathfrak{h}_j^k$  and  $\text{PL}_j^k$  are the channel fading gain and path loss for the LoS (L) and Non-Line-of-Sight (NLoS) (N) links, respectively. Finally, in Eq. (1),  $G_{\text{gNB},k}$  ( $G_{\text{UE}}$ ) represents the beamforming gain at the gNB (UE) towards (of) the  $k$ -th user. We assume analog beamforming (a realistic assumption for RedCap devices to minimize energy consumption [29]) at the gNB, which can thus probe only one direction at a time. Specifically, the gNB is equipped with a uniform linear antenna array with  $N_{\text{gNB}}$  elements, so the beamforming gain is expressed as [30]

$$G_{\text{gNB},k} = \left| \sin \left( \frac{\pi N_{\text{gNB}}}{2} \sin \theta_k \right) / \sin \left( \frac{\pi}{2} \sin \theta_k \right) \right|, \quad (3)$$

where  $\theta_k$  is the angular offset with respect to  $\text{UE}_k$ , as described in Sec. II-D. Moreover, we assume that UEs are equipped with a single isotropic antenna to promote energy efficiency, i.e.,  $G_{\text{UE}} \equiv 1$ .

### B. Beam Management Model

According to the 5G NR specifications [2], beam management relies on a directional version of the 4G LTE synchronization signal called SSB. Specifically, each SSB consists of 4 OFDM symbols in time and 240 subcarriers in frequency, where the subcarrier spacing depends on the 5G NR numerology [20]. Each SSB is mapped into a certain angular direction so that directional measurements can be made based on the quality of the received signal, e.g., in terms of the SNR. To reduce the overhead, SSBs are grouped into SS bursts, which consist of  $N_{\text{SS}} \in \{8, 16, 32, 64\}$  SSBs, contiguous in time. The periodicity between consecutive SS bursts is  $T_{\text{SS}} \in \{5, 10, 20, 40, 80, 160\}$  ms.

### C. Energy Consumption Model

In 5G NR beam management, the gNB transmits the SSBs by sequentially sweeping different angular directions to cover the whole beam space (or cell sector). The transmission of these control signals entails an energy consumption at the gNB which can be expressed as

$$E_C = S_D P_{\text{gNB}} T_{\text{SSB}}, \quad (4)$$

where  $S_D$  is the number of SSBs required to completely sweep the beam space (which is a function of the beamwidth at the

TABLE I  
POWER CONSUMPTION PARAMETERS.

Parameter	Description	Value
$P_{PS}$	Phase shifter	21.6 mW
$P_M$	Mixer	0.3 mW
$P_{LO}$	Local oscillator	22.5 mW
$P_{LPF}$	Low pass filter	14 mW
$P_{BB}$	Baseband amplifier	5 mW
$P_{DAC}$	DAC	[31, Eq. (13)]

gNB),  $P_{\text{gNB}}$  is the power consumed for transmitting each SSB, and  $T_{\text{SSB}}$  is the time required to send each SSB.

From [20, Eq. (3)],  $S_D$  relative to the horizontal plane (with azimuth ranging from 0 to  $2\pi$ ) can be expressed as

$$S_D = \lceil 2\pi/\Delta_{3\text{dB}} \rceil \approx \lceil \pi N_{\text{gNB}} \rceil, \quad (5)$$

where  $\Delta_{3\text{dB}} \approx 2/N_{\text{gNB}}$  is the 3-dB beamwidth [30]. Since each SSB consists of 4 OFDM symbols, the time (in  $\mu\text{s}$ ) required to send one SSB can be expressed as [20, Eq. (2)]

$$T_{\text{SSB}} = 4T_{\text{symlb}} = 4(71.45/2^n), \quad (6)$$

where  $n$  represents the 5G NR numerology index.

The transmitter RF front-end for analog beamforming consists of a pair of Digital-to-Analog Converters (DACs) (one for each I/Q channel), one RF chain, a Local Oscillator (LO), a Power Amplifier (PA), and  $N_{\text{gNB}}$  Phase Shifters (PSs). According to [31], the total power consumption at the transmitter is thus given by

$$P_{\text{gNB}} = N_{\text{gNB}}P_{\text{PS}} + P_{\text{PA}} + P_{\text{RF}} + P_{\text{LO}} + 2P_{\text{DAC}}, \quad (7)$$

where  $P_{\text{RF}} = 2P_M + 2P_{\text{LPF}}$  is the power consumption of the RF chain, and  $P_{\text{PA}}$  stands for the power consumed by the power amplifier. In turn,  $P_{\text{PA}}$  can be expressed as  $P_{\text{PA}} = P_T/\eta$ , where  $\eta$  is the power-added efficiency [32].  $P_{\text{DAC}}$  denotes the power consumption of a DAC, and can be computed as [31, Eq. (13)]

$$P_{\text{DAC}} = 1.5 \times 10^{-5} 2^{b_{\text{DAC}}} + 9 \times 10^{-12} b_{\text{DAC}} F_s, \quad (8)$$

where  $F_s$  is the sampling frequency and  $b_{\text{DAC}}$  is the number of resolution bits. A thorough description of the power components appearing in Eq. (7), and the corresponding numerical values used in this work, is provided in Table I.

#### D. Beam Dynamics Model

At first,  $\text{UE}_k$ ,  $k \in \{1, 2, \dots, K\}$ , establishes an initial connection with the gNB using beam

$$m_{i,k} = \arg \min_m (\phi_k - \phi_{br,m}), \quad m \in \{1, 2, \dots, S_D\}, \quad (9)$$

where  $\phi_{br,m} \equiv (m-1)\Delta_{3\text{dB}}$  is the antenna boresight direction of the  $m$ -th beam. Due to the finite nature of the pre-defined codebook of directions available at the gNB,  $\text{UE}_k$  thus comes with a non-zero initial angular offset

$$\theta_{i,k} = \phi_k - \phi_{br,m_{i,k}} \quad (10)$$

with respect to the boresight direction of the  $m_{i,k}$ -th beam, as represented in Fig. 1.

Moreover, we assume that during beam management  $\text{UE}_k$  moves with a tangential speed  $v$ . Therefore, during the time in between beam updates,  $\text{UE}_k$  progressively loses beam alignment, and so the resulting beamforming gain starts to deteriorate. Eventually,  $\text{UE}_k$  may also end up in the coverage region of a different beam, and possibly get disconnected whenever the resulting SNR is below a given threshold [33]. To account for this misalignment, we define  $\theta_{v,k}$ , also represented in Fig. 1, as the angular offset accumulated due to the movement of  $\text{UE}_k$  in between consecutive beam updates, i.e.,

$$\theta_{v,k} = vT_{\text{BM}}/d_k. \quad (11)$$

In Eq. (11),  $T_{\text{BM}}$  is the beam management time, i.e., the time it takes to send SSBs across all the  $S_D$  angular directions, which in turn can be expressed as [20, Eq. (4)]

$$T_{\text{BM}} = T_{\text{SS}} (\lceil S_D/N_{\text{SS}} \rceil - 1) + T_\ell, \quad (12)$$

where  $T_\ell$  is the time required to send the remaining SSBs in the last burst, and is given in [20, Eq. (6)].

Therefore, the overall angular offset for  $\text{UE}_k$  during beam management due to both the initial offset and the offset accumulated due to mobility can be expressed as

$$\theta_k = |\theta_{i,k} + \theta_{v,k}|. \quad (13)$$

### III. ENERGY CONSUMPTION OPTIMIZATION PROBLEM

In Sec. III-A we define an optimization problem P1 to minimize the energy consumption of beam management at the UAV-gNB by tuning both the transmission power and the beamwidth at the gNB, while ensuring a sufficient link quality. Moreover, in Sec. III-B we generalize the problem to an arbitrary misdetection probability (P2). Finally, in Sec. III-C we present our optimization algorithm to solve P1 and P2.

#### A. Baseline Optimization Problem

The baseline optimization problem (P1) is formalized as

$$\text{P1} : \min_{N_{\text{gNB}}, P_t} E_C = S_D P_{\text{gNB}} T_{\text{SSB}}, \quad (14)$$

$$C_1 : P_t \gamma_k \geq \tau, \quad \forall k,$$

$$C_2 : 0 < P_t \leq P_T,$$

$$C_3 : N_{\text{gNB}} \in \{i \in \mathbb{N} \mid i \leq 64\}.$$

Constraint  $C_1$  ensures that the transmission power  $P_t$  at the gNB is such that the SNR of each user is greater than or equal to a given threshold  $\tau$ , so UEs can be properly detected.  $C_2$  stipulates that  $P_t$  be less than or equal to the maximum transmission power  $P_T$ , whereas  $C_3$  sets the upper bound of the number of antennas at the gNB to 64, in line with RedCap design guidelines [15].

Basically, the above optimization problem determines the optimal values of  $N_{\text{gNB}}$  and  $P_t$ , referred to as  $N_{\text{gNB}}^*$  and  $P_t^*$ , such that  $E_C$  is minimized, and the SNR of each UE is greater than a threshold  $\tau$ . From Eq. (1),  $\gamma_k$  depends on  $G_{\text{gNB}}$ , and hence on the angular offset  $\theta_k$  between the UEs and the boresight of the corresponding serving beam. In turn, the misalignment is a function of: (i) the UE velocity  $v$  (the faster the UE, the sooner it loses alignment); (ii) the beam management time  $T_{\text{BM}}$  and, consequently  $T_{\text{SS}}$  and  $N_{\text{SS}}$

(the slower the beam management procedure, the higher the probability that a UE loses alignment); and (iii) the number of antennas  $N_{\text{gNB}}$ , which in turn determines the beamwidth (the narrower the beam, the smaller the angular offset, which leads to a beamforming gain degradation). In the remainder of this work, we investigate the impact of these parameters on the above optimization problem.

### B. Generalized Optimization Problem: Non-Zero Misdetection

In Eq. (14),  $C_1$  enforces that no UE violates the SNR constraint. To further generalize the problem, we also consider the case where some UEs are allowed to violate  $C_1$  even though, statistically, most of the UEs experience a sufficient link quality. To this end, we introduce the misdetection probability  $P_{\text{MD}}$ , and define an additional optimization problem which optimizes  $N_{\text{gNB}}$  and  $P_t$  while ensuring that *at least*  $(1 - P_{\text{MD}})K$  users, out of  $K$  UEs, experience a sufficient SNR.

The generalized problem (P2) can be formalized as

$$\begin{aligned} \text{P2 : } \min_{N_{\text{gNB}}, P_t} \quad & E_C = S_D P_{\text{gNB}} T_{\text{SSB}}, \quad (15) \\ & C'_1 : \mathbb{P}_k[P_t \gamma_k \geq \tau] \geq 1 - P_{\text{MD}}, \\ & C_2 : 0 < P_t \leq P_T, \\ & C_3 : N_{\text{gNB}} \in \{i \in \mathbb{N} \mid i \leq 64\}. \end{aligned}$$

where  $C'_1$  ensures that the probability that UE $_k$  satisfies the SNR constraint is greater than or equal to  $1 - P_{\text{MD}}$ . In other words,  $C'_1$  allows the problem to be feasible even if  $K P_{\text{MD}}$  UEs lose alignment with the associated beam.

### C. Optimization Algorithm

Due to the multiple nonlinearities in P1, such as the nested ceiling function and the dependence of  $C_1$  on the integer  $N_{\text{gNB}}$ , the optimization problem in Eq. (14) is a Mixed-Integer Nonlinear Program (MINLP), and thus non-convex. In fact, even powerful conventional solvers such as MATLAB's `surrogateopt`, and GAMS' `ANTIGONE` [34] and GUROBI [35] failed to solve it. Therefore, we develop and present an MC algorithm, reported in Alg. 1, for obtaining the optimal solution of P1.

The algorithm is designed with the following rationale. First, it can be observed that Eq. (4) can be lower bounded as

$$(4) \geq 3T_{\text{SSB}} N_{\text{gNB}} \left( P_t / \eta + N_{\text{gNB}} P_{\text{PS}} + P'_{\text{RF}} \right), \quad (16)$$

where  $P'_{\text{RF}} = P_{\text{RF}} + P_{\text{LO}} + 2P_{\text{LDAC}}$ . So, the derivatives of  $E_C$  with respect to  $P_t$  and  $N_{\text{gNB}}$  are non-negative, i.e.,

$$\frac{\partial E_C}{\partial N_{\text{gNB}}} \geq 3T_{\text{SSB}} \left( \frac{P_t}{\eta} + 2N_{\text{gNB}} P_{\text{PS}} + P'_{\text{RF}} \right) > 0, \quad (17)$$

$$\frac{\partial E_C}{\partial P_t} \geq \frac{3T_{\text{SSB}} N_{\text{gNB}}}{\eta} > 0, \quad (18)$$

since feasible values of  $N_{\text{gNB}}$  are strictly positive (as per  $C_3$ ). Therefore, it can be concluded that the objective function drives the optimization problem to choose the minimum values of  $N_{\text{gNB}}$  and  $P_t$  that meet the SNR constraint.

---

### Algorithm 1: Computation of the solution of Eq. (14).

---

```

1 Initialize  $P_T, \tau, K, R$ ;
2 for each iteration  $j = 1, \dots, N_{\text{MC}}$  do
3   for each UE  $k = 1, \dots, K$  do
4      $\phi_k \leftarrow 2\pi \text{rand}(1)$ ;
5      $d_k \leftarrow R\sqrt{\text{rand}(1)}$ ;
6   end
7   for  $N_{\text{gNB}} = 1, 2, \dots, 64$  do
8      $S_D = \lceil \pi N_{\text{gNB}} \rceil, \Delta_{3\text{dB}} = 2/N_{\text{gNB}}$ ;
9     for each UE  $k = 1, \dots, K$  do
10      Compute  $\gamma_k, \theta_{i,k}, \theta_{v,k}$ , and  $\theta_k$ , using
11      Eqs. (1), (10), (11), and (13), respectively;
12    end
13    if  $P_T \gamma_k \geq \tau \forall \text{ UE } k$  then
14       $N_j^* \leftarrow N_{\text{gNB}}$ ;
15       $P_{t,j}^* \leftarrow \tau / \min_k \gamma_k$ ;
16      break;
17    end
18  end
19  $N_{\text{gNB}}^* = \sum_{i=j}^{N_{\text{MC}}} N_j^* / N_{\text{MC}}$ ;
20  $P_t^* = \sum_{i=j}^{N_{\text{MC}}} P_{t,j}^* / N_{\text{MC}}$ ;

```

---

By further inspecting Eqs. (4), (5), and (7), we see that  $E_C$  exhibits a quadratic dependence with respect to  $N_{\text{gNB}}$ , and a linear dependence with respect to  $P_t$ . Therefore, we infer that  $N_{\text{gNB}}$  is the asymptotically dominant variable in the optimization problem.<sup>3</sup> This suggests that the minimum value of  $N_{\text{gNB}}$  for which  $C_1$  is satisfied, assuming  $P_t = P_T$ , is the optimal  $N_{\text{gNB}}$ , i.e.,  $N_{\text{gNB}}^*$ . Then, once  $N_{\text{gNB}}^*$  is fixed, the optimal transmission power  $P_t^*$  can be computed as the minimum value which satisfies  $C_1$  for  $N_{\text{gNB}} = N_{\text{gNB}}^*$ , i.e.,  $P_t^* = \tau / \min_k \gamma_k$ . Finally, whenever for a given value of  $P_T$  and  $\tau$  the constraints cannot be met with any feasible value of  $N_{\text{gNB}}$ , the problem is assumed to be infeasible.

To generalize the algorithm for solving P2, we simply modify the condition of Line 12 in Alg. 1 as

$$\sum_{k=1}^K \mathbb{1}(P_t \gamma_k \geq \tau) \geq (1 - P_{\text{MD}})K, \quad (19)$$

and the condition of Line 14 as

$$P_t^* \leftarrow \tau / \lceil \gamma \rceil_{\lceil (1 - P_{\text{MD}})K \rceil}, \quad (20)$$

where  $\gamma$  is the vector of the SNR values  $\gamma_k$ , sorted in descending order, and  $\lceil \gamma \rceil_i$  is the  $i$ -th entry of  $\gamma$ .

## IV. OPTIMIZATION METRICS

Based on the optimization problem in Sec. III, we introduce and formalize two fundamental optimization metrics that will be used to evaluate and dimension RedCap beam management, namely the average angular offset (Sec. IV-A) and the feasibility regions (Sec. IV-B).

### A. Angular Offset

The first optimization metric that we consider for evaluating the solutions of P1 and P2 is the average angular offset  $\bar{\theta}$  of all

<sup>3</sup>The dominance of  $N_{\text{gNB}}$  with respect to  $P_t$  has been verified experimentally for practical values of the problem parameters.

$$\bar{\theta} = \int_0^R \int_{-\frac{\Delta_{3dB}}{2}}^{\frac{\Delta_{3dB}}{2}} \left| x + \frac{vT_{SS} (\lceil \lceil \pi N_{gNB} \rceil / N_{SS} \rceil - 1) + T_\ell}{y} \right| \frac{2y}{R^2} \frac{N_{gNB}}{2} dx dy. \quad (21)$$

$K$  UEs in the region. Since users are uniformly distributed in the circular area, the probability density functions of the initial phase  $\phi_k$  and distance  $d_k$  relative to the center are respectively written as

$$p_{\phi_k}(x) = \begin{cases} \frac{1}{2\pi} & \text{if } x \in [0, 2\pi) \\ 0 & \text{otherwise,} \end{cases} \quad (22)$$

$$p_{d_k}(x) = \begin{cases} \frac{2x}{R^2} & \text{if } x \in [0, R] \\ 0 & \text{otherwise.} \end{cases} \quad (23)$$

For a given number of antennas  $N_{gNB}$ , the serving region is subdivided into  $S_D$  regions of equal area. Since  $\phi_k$  is uniformly distributed, UE $_k$  is under the initial coverage of beam  $m \in \{1, \dots, S_D\}$  with probability  $\mathbb{P}(m) = 1/S_D$ . Therefore, the probability density function of the initial offset  $\theta_{i,k}$  with respect to the boresight direction of beam  $m$  is

$$p_{\theta_{i,k}}(x | m) = \begin{cases} 1/\Delta_{3dB} & \text{if } x \in [-\Delta_{3dB}/2, \Delta_{3dB}/2] \\ 0 & \text{otherwise.} \end{cases}$$

Then, the average angular offset  $\bar{\theta}$  can be expressed as

$$\bar{\theta} = \sum_{m=1}^{S_D} \mathbb{E}[\theta | m] \mathbb{P}(m) \quad (24)$$

$$= \sum_{m=1}^{S_D} \mathbb{E}[\theta | m] (1/S_D) = \mathbb{E}[\theta | m], \quad (25)$$

so  $\bar{\theta}$  does not depend on the specific beam  $m$ . Therefore,  $\bar{\theta}$  can be evaluated by focusing on the coverage region of a single beam as

$$\bar{\theta} = \mathbb{E}[|\theta_{i,k} + \theta_{v,k}| | m] \quad (26)$$

$$= \int_0^R \int_{-\frac{\Delta_{3dB}}{2}}^{\frac{\Delta_{3dB}}{2}} |\theta_{i,k} + \theta_{v,k}| p(x)_{\theta_{i,k}} p(y)_{d_k} dx dy \quad (27)$$

$$= \int_0^R \int_{-\frac{\Delta_{3dB}}{2}}^{\frac{\Delta_{3dB}}{2}} \left| x + \frac{vT_{BM}}{y} \right| \frac{2y}{R^2} \frac{1}{\Delta_{3dB}} dx dy. \quad (28)$$

Rendering explicit the dependence on  $N_{gNB}$ ,  $N_{SS}$  and  $T_{SS}$ , Eq. (28) can be further manipulated into Eq. (21).

### B. Feasibility Regions

Given the maximum transmission power  $P_T$ , the SNR threshold  $\tau$ , and the number of users  $K$ , P1 and P2 yield the optimal number of antennas  $N_{gNB}^*$  and transmission power  $P_t^*$  at the gNB. Based on these values, we determine the upper limits of the ground speed  $v$  and the burst periodicity  $T_{SS}$  which prevent the misalignment of the UEs with respect to the corresponding associated beam. To this end, we define the alignment condition of UE $_k$ , with initial (accumulated) offset

TABLE II  
SIMULATION PARAMETERS.

Parameter	Description	Value
$h_{gNB}$	gNB height	35 m
$h_{UE}$	UE height	1.5 m
$R$	Radius of the SmA scenario	100 m
$K$	Number of UEs	{50, 100, 200, 500, 1000}
$f_c$	Carrier frequency	28 GHz
$B$	Bandwidth	50 MHz
$h_{LoS}^k, h_{NLoS}^k$	Channel fading gains	$\mathcal{CN}(0, 1)$
$PL_{LoS}^k, PL_{NLoS}^k$	Path loss	[27, Table 7.4.1-1]
$P_r(d_{3D})$	LoS probability	[27, Table 7.4.2-1]
$N_0$	Noise PSD	-174 dBm/Hz
$n$	5G NR numerology index	4
$N_{MC}$	Number of MC simulations	$10^5$
$\eta$	Power added efficiency	27%
$b_{DAC}$	DAC bit resolution	8
$F_s$	DAC sampling frequency	$10^9$ Hz
$T_{SS}$	SS burst period	{5, 10, 20, 40, 80, 160} ms
$N_{SS}$	Number of SSBs per burst	{8, 16, 32, 64}
$v$	UE speed	[1, 30] m/s
$P_T$	Maximum transmission power	[10, 40] dBm
$\tau$	SNR threshold	[1, 10] dB

$\theta_{i,k}(\theta_{v,k})$ , as being located within the angular coverage region of its associated beam. This can be formalized as

$$\theta_{i,k} + \theta_{v,k} \leq \frac{\Delta_{FNBW}}{2}, \quad (29)$$

where  $\Delta_{FNBW} = 2 \sin^{-1} [2/N_{gNB}^*]$  is the First Null Beam Width (FNBW). Therefore, Eq. (29) bounds the maximum angular offset to the first null beamwidth, i.e., the angular region between the first zeros of the main lobe.

Given the independence of  $\theta_{i,k}$  and  $\theta_{v,k}$ , and substituting the expression of  $\theta_{v,k}$  from Eq. (11), we get

$$\theta_{i,k} + \frac{vT_{SS}}{d_k} \left( \left\lceil \frac{S_D}{N_{SS}} \right\rceil - 1 \right) \leq \frac{\Delta_{FNBW}}{2},$$

which can be further manipulated into

$$vT_{SS} \leq d_k \left[ \frac{\Delta_{FNBW}/2 - \theta_{i,k}}{\left( \lceil S_D/N_{SS} \rceil - 1 \right)} \right], \quad (30)$$

thus providing an upper limit for the feasible product of  $v$  and  $T_{SS}$  for given values of  $N_{gNB}^*$ ,  $N_{SS}$ , and  $K$ . Finally, Eq. (30) can be evaluated by substituting the random quantities  $d_k$  and  $\theta_{i,k}$  with their deterministic worst-case counterparts, and taking the value of  $\Delta_{FNBW}$  which corresponds to the highest possible gain, i.e.,

$$vT_{SS} \leq \min_k d_k \left[ \frac{\Delta_{FNBW}/2 - \max_k \theta_{i,k}}{\left( \lceil S_D/N_{SS} \rceil - 1 \right)} \right]. \quad (31)$$

## V. NUMERICAL RESULTS

In this section we numerically evaluate the optimal number of antennas  $N_{gNB}^*$  and transmission power  $P_t^*$  to minimize  $E_C$  during beam management in different system configurations, for  $N_{MC} = 10^5$  Monte Carlo simulations. We study the impact of the beam management parameters, the maximum transmission power, the SNR threshold, and the number of users on

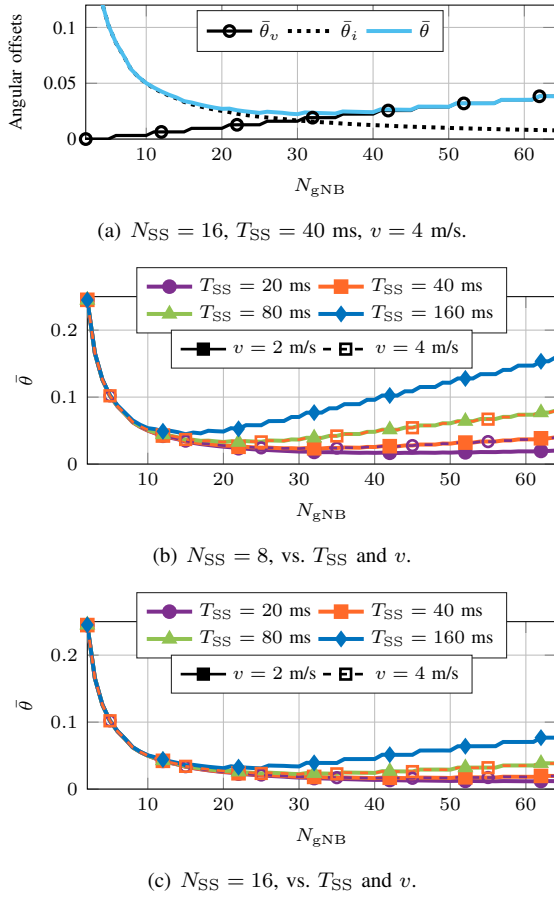


Fig. 2. Average angular offset  $\bar{\theta}$  as a function of  $N_{gNB}$ ,  $v$ , and  $T_{SS}$ . In the two bottom figures, solid lines and filled markers represent  $v = 2$  m/s, while dashed lines and empty markers represent  $v = 4$  m/s.

the solution of P1, and compare it with the solution of P2 when the misdetection probability is not zero. Moreover, we evaluate the feasible angular offsets, and define the feasibility regions for RedCap devices, which strike an optimal trade-off between QoS and  $E_C$ .

In our simulations, we used the 3GPP LoS probability and path loss parameters for RMA scenarios reported in [27, Tables 7.4.1-1, 7.4.2-1]. The parameters for the UEs and gNB are from the RedCap design guidelines [15], while the power consumption parameters are taken from [31], as summarized in Table II.

### A. Angular Offset

In Fig. 2 we plot the angular offset  $\bar{\theta}$  averaged over all  $K$  UEs in the region, versus  $N_{gNB}$ , and for different values of  $v$ ,  $N_{SS}$  and  $T_{SS}$ . Notice that  $\bar{\theta}$  depends on the average initial offset  $\bar{\theta}_i$  and the average offset due to mobility  $\bar{\theta}_v$ . As depicted in Fig. 2(a), the former decreases monotonically with  $N_{gNB}$  since the beamwidth  $\Delta_{3dB}$  and hence the angular distance between consecutive boresight directions decrease. Conversely, the latter increases (through not monotonically due to the ceiling function in Eq. (11)) with  $N_{gNB}$  since the number of SSBs required for a complete beam scan increases. Overall,  $\bar{\theta}$  decreases and then increases with  $N_{gNB}$ .

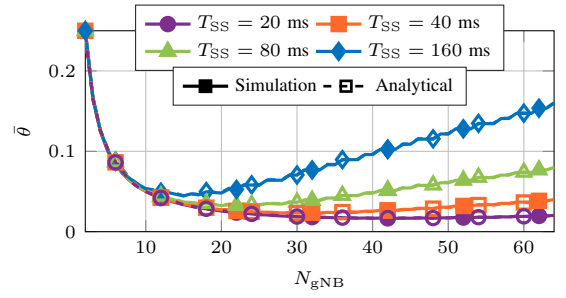
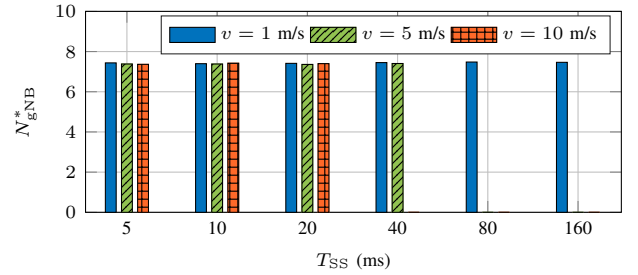


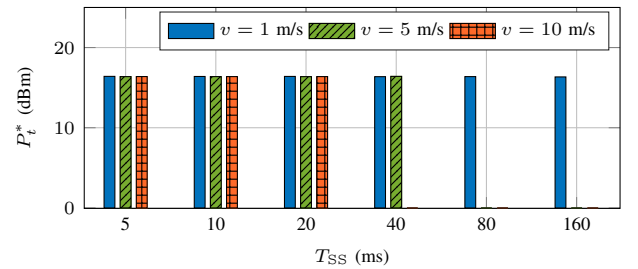
Fig. 3. Average angular offset  $\bar{\theta}$  obtained from Eq. (21) (dashed lines and empty markers) and via Monte Carlo simulation (solid lines and filled markers), as a function of  $N_{gNB}$  and  $T_{SS}$ , for  $v = 2$  m/s and  $N_{SS} = 8$ .

When the number of antennas is small, e.g., for  $N_{gNB} \leq 10$ , beams are sufficiently large to ensure continuous alignment of the UEs, despite their mobility. In this case,  $\bar{\theta}$  is dominated by the initial offset  $\bar{\theta}_i$ , so  $\bar{\theta}$  decreases with  $N_{gNB}$  as reported in Fig. 2(b). As  $N_{gNB}$  increases, the beams become progressively narrower, and the number of SSBs that are required to exhaustively scan the angular space increases. As such, the beam management time increases as per Eq. (11), so  $\bar{\theta}$  is dominated by  $\bar{\theta}_v$ , and the impact of  $v$  is non-negligible.

From Figs. 2(b) and 2(c) we further observe that  $\bar{\theta}$  grows with  $v$  and  $T_{SS}$  when  $N_{gNB} \geq 10$ , even though this effect can be partially mitigated by increasing  $N_{SS}$ . Additionally, we observe that the angular offset for  $v = 4$  m/s and  $T_{SS} = 20$  ms is equal to the offset for  $v = 2$  m/s and  $T_{SS} = 40$  ms. Similarly, the offset for  $v = 4$  m/s and  $T_{SS} = 40$  is equal to the offset for  $v = 2$  m/s and  $T_{SS} = 80$  ms. Therefore, we conclude that  $\bar{\theta}$  depends on  $v$  and  $T_{SS}$  only through their product, an observation which will be particularly relevant for the analysis of the feasibility regions in Sec. V-F.



(a) Optimal number of antenna elements  $N_{gNB}^*$  at the gNB.



(b) Optimal transmission power  $P_t^*$  at the gNB.

Fig. 4.  $N_{gNB}^*$  and  $P_t^*$  as a function of  $v$  and  $T_{SS}$ , for  $N_{SS} = 8$ ,  $P_T = 18$  dBm,  $\tau = 7$  dB, and  $K = 50$ . Missing values represent infeasibility.



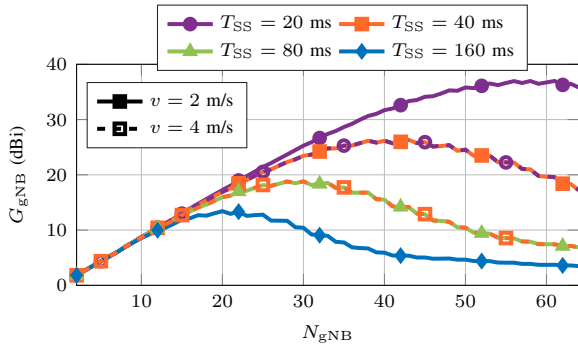


Fig. 5. Average beamforming gain  $G_{\text{gNB}}$  at the gNB as a function of  $N_{\text{gNB}}$ ,  $v$  and  $T_{\text{SS}}$ , for  $N_{\text{SS}} = 8$ . Solid lines and filled markers represent  $v = 2$  m/s, while dashed lines and empty markers represent  $v = 4$  m/s.

In Fig. 3 we also report the average angular offset obtained both via Monte Carlo simulations and by evaluating the analytical expression in Eq. (21). We can see that the curves perfectly match, thus validating our analytical results.

*Summary:* The angular offset depends on the product of  $v$  and  $T_{\text{SS}}$ , and is non-monotonic with respect to  $N_{\text{gNB}}$ . In particular, the angular offset is dominated by the initial angular offset when  $N_{\text{gNB}}$  is small, and then by the angular offset due to mobility when  $N_{\text{gNB}}$  increases.

### B. Impact of the Beam Management Parameters

Fig. 4 depicts  $N_{\text{gNB}}^*$  and  $P_t^*$  as a function of  $T_{\text{SS}}$  and  $v$ , for  $N_{\text{SS}} = 8$ ,  $P_T = 18$  dBm,  $\tau = 7$  dB, and  $K = 50$ .<sup>4</sup> We observe that the values of  $N_{\text{gNB}}^*$  and  $P_t^*$  do not change much with respect to both  $v$  and  $T_{\text{SS}}$  at  $N_{\text{SS}} = 8$ . This is motivated by the fact that the objective function drives the optimization problem towards the minimum values of  $N_{\text{gNB}}^*$  and  $P_t^*$  that meet the SNR constraint, so as to minimize  $E_C$ . Therefore,  $N_{\text{gNB}}^*$  takes the minimum value corresponding to the largest offset beyond which the problem is infeasible, which also determines the corresponding values of  $v$  and  $T_{\text{SS}}$ . In the given configuration, we obtain  $N_{\text{gNB}}^* = 7.4$  and  $P_t^* = 16.4$  dBm. Notice that some bars are missing in Fig. 4, e.g., for  $v \geq 5$  m/s when  $T_{\text{SS}} \geq 80$  ms and  $N_{\text{SS}} = 8$ , which indicates that the problem is infeasible. That is to say, for given values of  $P_T$  and  $\tau$ , only some values of  $v$  and  $T_{\text{SS}}$  are feasible.

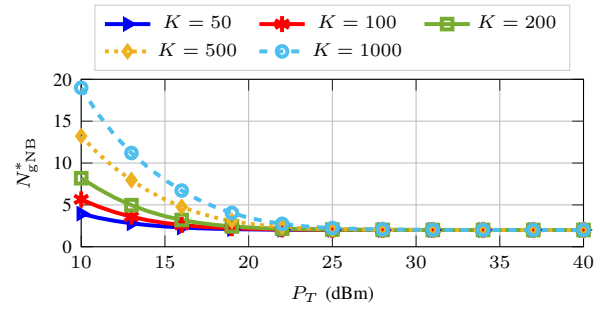
Moreover, as depicted in Fig. 5, the beamforming gain  $G_{\text{gNB}}$  is approximately constant with respect to  $v$  and  $T_{\text{SS}}$ , as long as  $N_{\text{gNB}}$  is small (approximately,  $N_{\text{gNB}} < 10$ ). In this case, misalignment is mainly due to the initial offset (see Sec. V-A), which does not depend on  $v$  or  $T_{\text{SS}}$ .

*Summary:* The impact of  $T_{\text{SS}}$  and  $N_{\text{SS}}$  on  $N_{\text{gNB}}^*$  and  $P_t^*$  is negligible. Still, for given values of  $P_T$  and  $\tau$ , only some values of  $v$  and  $T_{\text{SS}}$  are feasible, where the constraints of P1 can be satisfied.

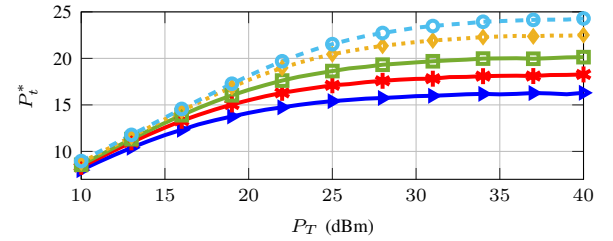
### C. Impact of the Maximum Transmission Power and the Number of Users

Fig. 6 depicts  $N_{\text{gNB}}^*$ ,  $P_t^*$ ,  $E_C$ , and  $P_C$  as a function of  $P_T$  and  $K$ . Specifically, we set  $\tau = -5$  dB, and consider

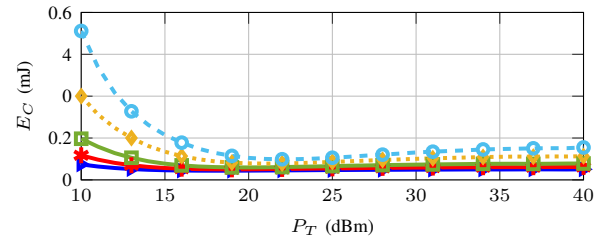
<sup>4</sup>We remark that, despite Constraint  $C_3$  in P1,  $N_{\text{gNB}}^*$  is possibly non-integer, since it represents the average value across several Monte Carlo realizations (see Line 19 in Alg. 1).



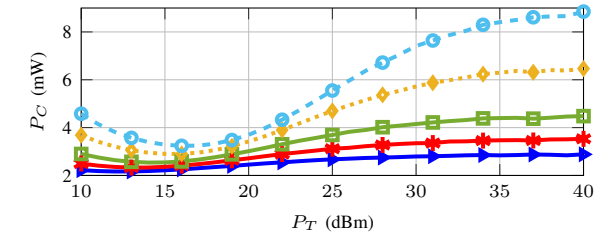
(a) Optimal number of antenna elements  $N_{\text{gNB}}^*$  at the gNB.



(b) Optimal transmission power  $P_t^*$  at the gNB.



(c) Energy consumption  $E_C$ .



(d) Power consumption  $P_C$ .

Fig. 6.  $N_{\text{gNB}}^*$ ,  $P_t^*$ ,  $E_C$ , and  $P_C$  as a function of  $P_T$  and  $K$ , for  $v = 1$  m/s,  $T_{\text{SS}} = 20$  ms,  $N_{\text{SS}} = 8$ , and  $\tau = -5$  dB.

values of  $P_T$  ranging from 10 to 40 dBm, while  $K \in \{50, 100, 200, 500, 1000\}$ . In Fig. 6(a) we observe that  $N_{\text{gNB}}^*$  decreases monotonically when increasing  $P_T$ , until a minimum value. This is because, by increasing the maximum transmission power (and so the SNR), thus relaxing Constraint  $C_2$ , we can safely decrease  $N_{\text{gNB}}^*$  (and so the energy consumption) while still satisfying Constraint  $C_1$ .

Conversely, Fig. 6(b) shows that  $P_t^*$  generally increases as  $P_T$  increases, until a maximum value after which  $P_t^*$  saturates, since higher transmission powers would only entail a higher  $E_C$ . This is explained by the fact that P1 yields the smallest value of  $P_t^*$  that meets Constraint  $C_1$  for  $N_{\text{gNB}}^*$ . For instance,  $C_1$  can be met for  $N_{\text{gNB}}^* = 2$  for  $P_T \geq 30$  dBm and  $K \leq 500$ .

Fig. 6(c) reports  $E_C$  as a function of  $K$  and  $P_T$ . We see



that  $E_C$  has a non-monotonic behavior with respect to  $P_T$ , so there exists an optimal value  $P_{T,E_C}^*$  that minimizes the energy consumption. We have that  $P_{T,E_C}^* \in \{18, 19, 20, 21, 22\}$  dBm for  $K \in \{50, 100, 200, 500, 1000\}$ , respectively. When  $P_T < P_{T,E_C}^*$ ,  $E_C$  is dominated by  $N_{\text{gNB}}^*$ : since the latter decreases with  $P_T$  (see Fig. 6(a)), so does  $E_C$ . On the other hand, when  $P_T > P_{T,E_C}^*$ ,  $P_t^*$  keeps increasing (see Fig. 6(b)) while  $N_{\text{gNB}}^*$  does not decrease further, so  $E_C$  eventually increases.

Finally, in Fig. 6(d) we plot the average power consumption  $P_C$  for sending SSBs over time. This is defined as the cumulative energy consumed for sending SSBs during a complete beam management sweep divided by its duration. It can be computed as

$$P_C = P_{\text{gNB}} T_{\text{SSB}} N_{\text{SS}} / T_{\text{SS}}, \quad (32)$$

where  $P_{\text{gNB}} T_{\text{SSB}}$  represents the energy consumed for sending one SSB as per Eq. (4). We observe that  $P_C$  has a similar shape as  $E_C$  since it also depends on both  $N_{\text{gNB}}^*$  and  $P_t^*$ , so there exists an optimal value  $P_{T,P_C}^*$  to minimize the power consumption. We have that  $P_{T,P_C}^* \in \{12, 13, 14, 16, 16\}$  dBm for  $K \in \{50, 100, 200, 500, 1000\}$ , respectively.

As expected, the impact of  $K$  is not negligible, and we have that both  $E_C$  and  $P_C$  increase as  $K$  increases. Moreover, as  $K$  decreases, the worst-case SNR increases, so  $N_{\text{gNB}}^*$  and  $P_t^*$  have to be higher too to satisfy the constraints in P1. Interestingly, when  $P_T$  is small,  $N_{\text{gNB}}^*$  increases quite rapidly with  $K$ , while the corresponding variation of  $P_t^*$  is negligible. This is because  $N_{\text{gNB}}^*$  has a larger impact on  $E_C$  than  $P_t^*$ .

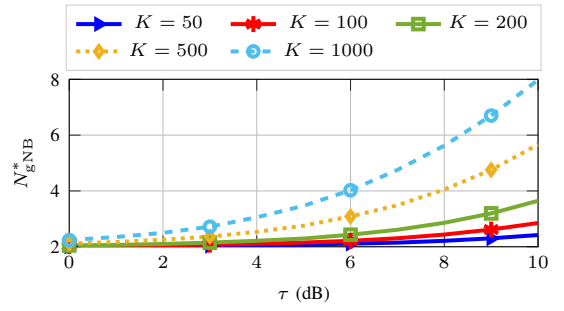
*Summary:*  $N_{\text{gNB}}^*$  and  $P_t^*$  monotonically decrease and increase with  $P_T$ , respectively. In turn, the shape of both  $E_C$  and  $P_C$  is non-monotonic, so there exists an optimal (intermediate) value of  $P_T$  to optimize the two. Finally, the impact of  $K$  is not negligible, and  $N_{\text{gNB}}^*$ ,  $P_t^*$ ,  $E_C$  and  $P_C$  increase as  $K$  increases.

#### D. Impact of the SNR Threshold and the Number of Users

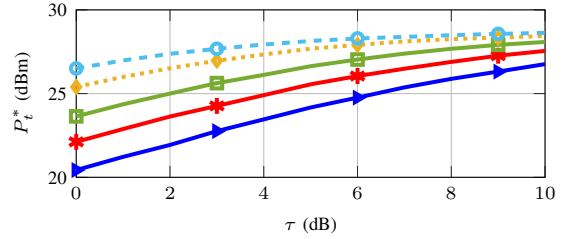
Fig. 7 reports  $N_{\text{gNB}}^*$ ,  $P_t^*$ ,  $E_C$ , and  $P_C$  as a function of  $\tau$  and  $K$ . We set  $P_T = 30$  dBm,  $\tau$  ranging from 0 to 10 dB, and  $K \in \{50, 100, 200, 500, 1000\}$ . Figs. 7(a) and 7(b) show that both  $N_{\text{gNB}}^*$  and  $P_t^*$  increase monotonically with respect to  $\tau$ . Similarly, Figs. 7(c) and 7(d) show that also  $E_C$  and  $P_C$  increase with  $\tau$ , and are minimized for  $\tau = 0$  dB. In fact, when  $\tau$  is small (so Constraint  $C_1$  is light), P1 yields the minimum value of  $N_{\text{gNB}}^*$  to minimize  $E_C$ , while  $P_t^*$  is large and already close to  $P_T$  to meet  $C_1$ . For instance, for  $\tau = 4$  dB and  $K = 500$ , we have  $N_{\text{gNB}}^* = 2.5$  and  $P_t^* \approx 27$  dBm. When  $\tau$  increases,  $P_t^*$  keeps increasing. Still, Constraint  $C_2$  upper bounds  $P_t^*$  to  $P_T$ , so  $P_t^*$  eventually saturates to  $P_T$ . In turn, P1 can only be solved by increasing  $N_{\text{gNB}}^*$ , at the expense of  $E_C$ .

Notice that the impact of a higher  $\tau$  is similar to that of a higher  $K$ , since both effectively require to either increase the beamforming gain (so increasing  $N_{\text{gNB}}^*$ ) or transmit with a higher power (so increasing  $P_t^*$ ) for P1 to be feasible.

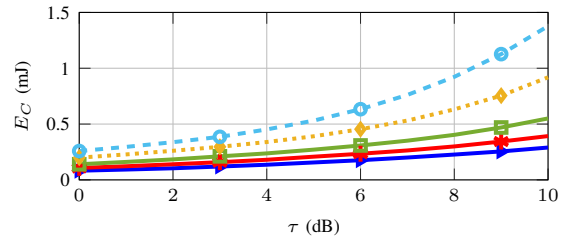
*Summary:*  $N_{\text{gNB}}^*$ ,  $P_t^*$ ,  $E_C$ , and  $P_C$ , monotonically increase with  $\tau$  since P1 is more constrained. The optimal strategy to minimize  $E_C$  is to minimize  $N_{\text{gNB}}^*$  first, and possibly increase  $P_t^*$  to meet the SNR constraint.



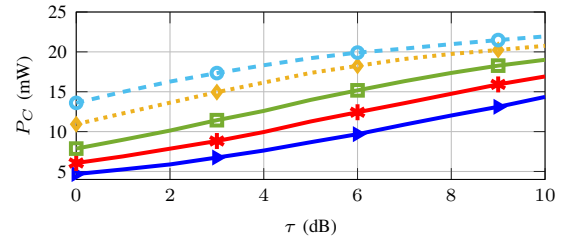
(a) Optimal number of antenna elements  $N_{\text{gNB}}^*$  at the gNB.



(b) Optimal transmission power  $P_t^*$  at the gNB.



(c) Energy consumption  $E_C$ .



(d) Power consumption  $P_C$ .

Fig. 7.  $N_{\text{gNB}}^*$ ,  $P_t^*$ ,  $E_C$ , and  $P_C$  as a function of  $\tau$  and  $K$ , for  $v = 1$  m/s,  $T_{\text{SS}} = 20$  ms,  $N_{\text{SS}} = 8$ , and  $P_T = 30$  dBm.

#### E. Joint Impact of the Transmission Power, the SNR Threshold, and the Number of Users

Fig. 8 depicts the joint impact of  $P_T$  and  $\tau$  on  $N_{\text{gNB}}^*$ ,  $P_t^*$ , and  $E_C$ . First, notice that some points are not defined since P1 is infeasible for certain values of  $P_T$  and  $\tau$ . For instance, for  $K = 50$  (i.e., with a UE density of  $0.0016/\text{m}^2$ ),  $P_T = 10$  dBm and  $\tau > 7$  dB are not feasible. For  $K = 1000$ , the feasibility domain is even smaller. For instance,  $P_T = 10$  dBm and  $\tau = 0$  dB are infeasible. This trend can be explained by the fact that, by increasing  $K$ , Constraint  $C_1$  must be satisfied for an increasing number of realizations.

Fig. 8(a) corroborates that  $N_{\text{gNB}}^*$  increases with  $\tau$  and decreases with  $P_T$ . Notably, the rate of increase of  $N_{\text{gNB}}^*$  with  $\tau$  is lower for higher values of  $P_T$ . In fact, when  $P_T$  is large,

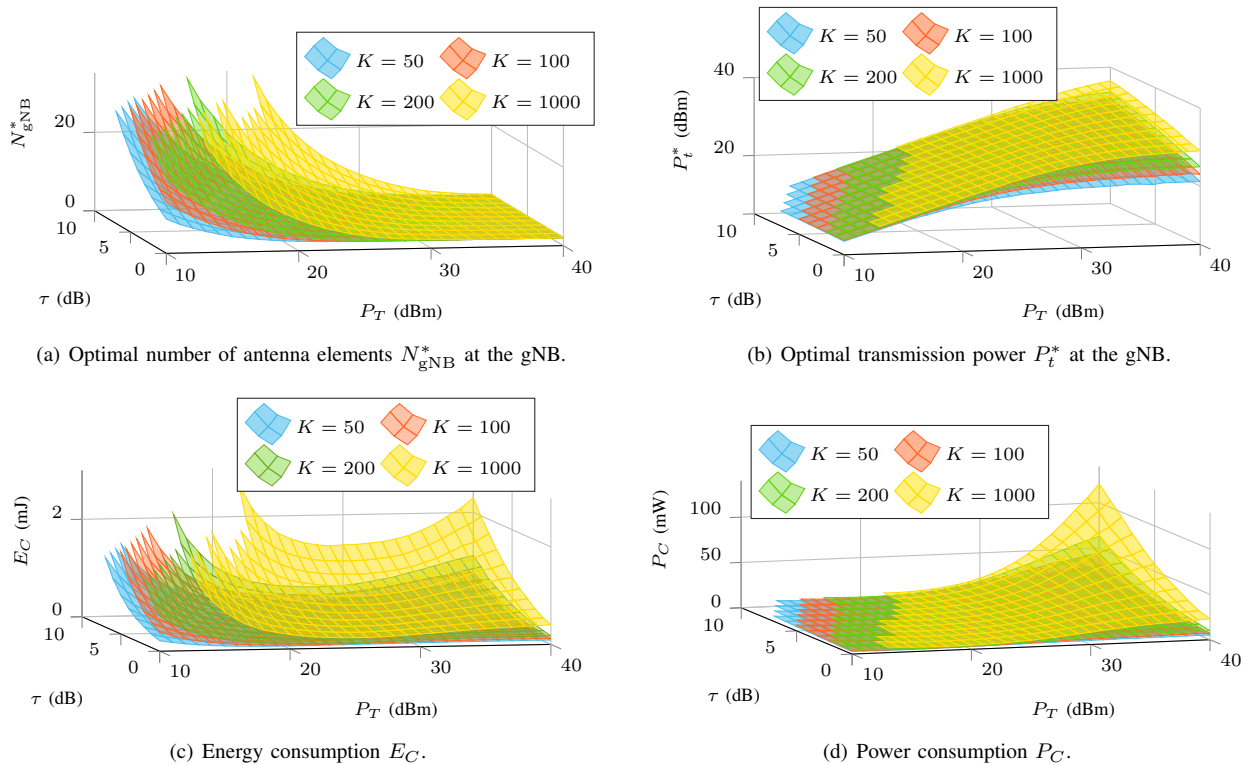


Fig. 8.  $N_{\text{gNB}}^*$ ,  $P_t^*$ ,  $E_C$ , and  $P_C$  as a function of  $P_T$ ,  $\tau$ , and  $K$ . Missing values represent infeasibility.

the system can easily satisfy the SNR constraint regardless of the value of  $N_{\text{gNB}}^*$ , so P1 is tempted to reduce  $N_{\text{gNB}}^*$  as much as possible to improve  $E_C$ . For example,  $N_{\text{gNB}}^* \approx 2$  for  $\tau = 10$  dB and  $P_T = 40$  dBm.

Similarly, Fig. 8(b) confirms that  $P_t^*$  increases with both  $P_T$  and  $\tau$ . In particular, P1 tends to yield the smallest possible value of  $P_t^*$  that satisfies  $C_1$  to minimize energy consumption, even though the gNB has to use more power when the system is more constrained, i.e., when  $\tau$  increases. Eventually, we observe that  $P_t^*$  saturates to  $P_T$  when  $\tau \geq 5$  dB.

Finally, Figs. 8(c) and 8(d) show that both  $E_C$  and  $P_C$  are non-monotonic with respect to  $P_T$ , while they both increase as  $\tau$  increases. The minimum  $E_C$  is observed for  $\tau = 0$  dB and  $P_T \in \{20, 22, 22, 26\}$  dBm for  $K \in \{50, 100, 200, 1000\}$ , respectively. On a similar note, the minimum  $P_C$  is observed for  $\tau = 0$  dB and  $P_T \in \{15, 15, 16, 18\}$  dBm for  $K \in \{50, 100, 200, 1000\}$ , respectively. Notably, these minimum points are independent of  $v$ ,  $T_{\text{SS}}$ , and  $N_{\text{SS}}$ .

*Summary:*  $N_{\text{gNB}}^*$ ,  $P_t^*$ ,  $E_C$  and  $P_C$  increase with  $\tau$ .  $N_{\text{gNB}}^*$  ( $P_t^*$ ) decreases (increases) with  $P_T$ , while  $E_C$  and  $P_C$  show a non-monotonic trend with respect to  $P_T$ .

#### F. Feasibility Regions

Based on the above discussion, we infer that, for each combination of  $P_T$  and  $\tau$ , there is a limit on the values of  $T_{\text{SS}}$ ,  $N_{\text{SS}}$ , and  $v$  for which the problem P1 (14) is feasible, that is when the SNR constraint is met. As described in Sec. IV-B, these values identify the so-called feasibility regions of P1, that is the set of feasible beam management parameters  $\{T_{\text{SS}}, N_{\text{SS}}\}$  for RedCap, and the corresponding maximum speed  $v$

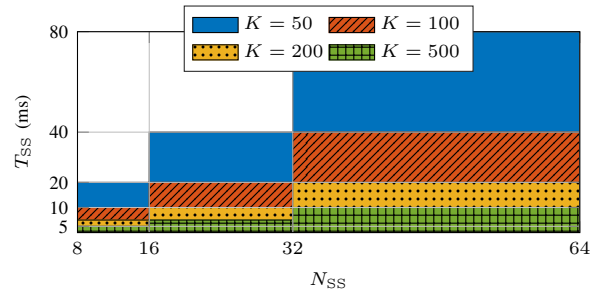


Fig. 9. Feasibility region for  $P_T = 18$  dBm,  $\tau = 7$  dB,  $v = 5$  m/s, for  $K \in \{50, 100, 200, 500\}$ .

and number of UEs  $K$  that can be tolerated. We recall that, as observed in Sec. V-A, the angular offset is defined in terms of the product of  $v$  and  $T_{\text{SS}}$ , so we characterize the shape of the feasibility regions also based on this product.

TABLE III  
FEASIBILITY REGIONS FOR  $P_T = 18$  DBM AND  $\tau = 7$  DB.

$N_{\text{SS}}$	$K$	Upper bound on $vT_{\text{SS}}$				
		50	100	200	500	1000
8		0.32 m	0.16 m	0.08 m	0.03 m	NF
16		0.64 m	0.32 m	0.16 m	0.06 m	NF
32		1.68 m	0.72 m	0.32 m	0.12 m	NF
64		4.80 m	1.76 m	0.64 m	0.32 m	NF

Specifically, Fig. 9 and Table III depict and report, respectively, the feasibility regions for  $P_T = 18$  dBm,  $\tau = 7$  dB,  $K \in \{50, 100, 200, 500, 1000\}$ , and considering  $v = 5$  m/s.

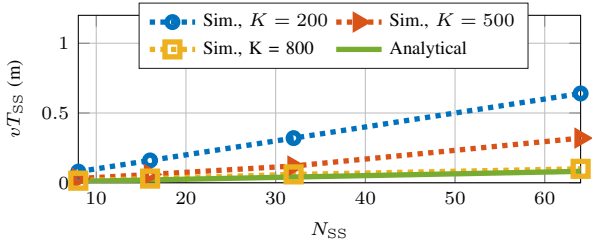


Fig. 10. Feasibility regions for  $P_T = 18$  dBm,  $\tau = 7$  dB, and  $v = 5$  m/s. Dashed lines are relative to the numerical results obtained via simulations for  $K \in \{50, 100, 200, 500\}$ , while the straight line represents the analytical feasibility lower bound for  $K \rightarrow +\infty$  based on Eq. (31).

We observe that the feasibility region becomes smaller, i.e., more values of  $v$  and  $T_{SS}$  become infeasible, as  $K$  increases. This is because increasing the number of UEs translates into a tighter constraint on the SNR ( $C_1$ ), so P1 tends to increase  $N_{\text{gNB}}^*$  to increase the beamforming gain. However, this also yields a narrower beam, thereby reducing the speed and the burst periodicity which can be sustained to avoid the misalignment of the UEs with respect to the corresponding associated beam.

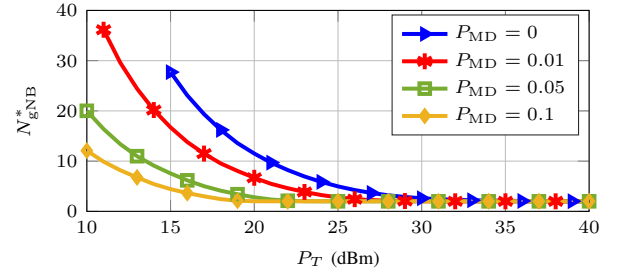
Fig. 10 compares the feasibility limits determined through numerical evaluation (and reported in Table III), and by using Eq. (31), for  $K \in \{200, 500, 800\}$ . We can see that Eq. (31), which effectively models the feasibility region for  $K \rightarrow \infty$ , provides a worst-case lower bound of the values obtained via simulation. As such, this bound is observed to be tight for  $K = 800$ , while instead there is a gap between the analytical model and the simulations as  $K$  decreases. This is due to the fact that, when  $K$  is small, the probability that a UE is located at the cell edge, and so measures an SNR which is close to that of the worst case, is small, so the corresponding feasibility regions are less constrained than those of the lower bound.

Finally, we observe that the size of the feasibility regions is inversely proportional to  $v$  and  $T_{SS}$ . Indeed, if the UEs move faster (i.e.,  $v$  increases), or if the beam management process takes longer (i.e.,  $T_{SS}$  increases), the probability that the UEs would lose beam alignment also increases. As such, the set of possible values of  $v$  and  $T_{SS}$  to make the problem feasible is smaller. Still, the impact of  $T_{SS}$  on the feasibility regions is zero for  $N_{SS} \geq S_D$ , i.e., if the transmission of the SSBs requires exactly one burst, as we can see from Eq. (12).

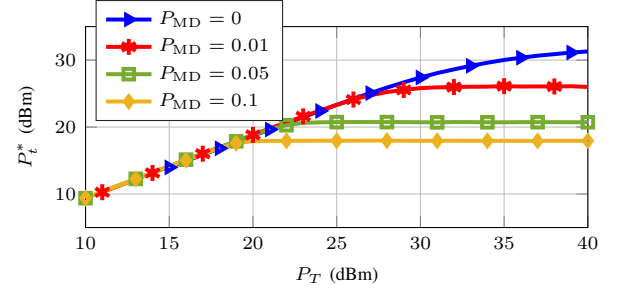
*Summary:* The size of the feasibility regions, i.e., the set of feasible values of RedCap beam management parameters  $\{T_{SS}, N_{SS}\}$ , depends on  $v$  and  $K$ . In any case, decreasing the beam management period, i.e., decreasing  $T_{SS}$  and maximizing  $N_{SS}$ , promotes feasibility.

### G. Arbitrary Misdetection Probability

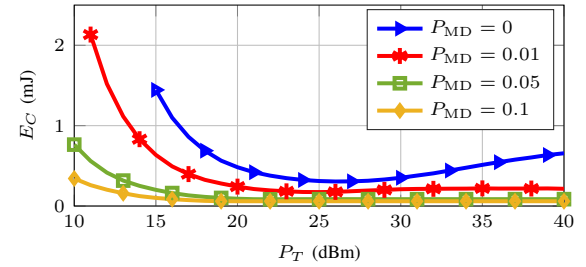
In this section we extend the previous analysis to P2, therefore exploring the impact of a non-zero misdetection probability ( $P_{\text{MD}} > 0$ ) on the optimal gNB configuration. In particular, Fig. 11 reports  $N_{\text{gNB}}^*$  and  $P_t^*$  as a function of  $P_T$ , for  $P_{\text{MD}}$  ranging from 0 to 0.1,  $v = 1$  m/s,  $T_{SS} = 20$  ms,  $N_{SS} = 8$ ,  $\tau = 7$  dB, and  $K = 200$ . Overall, it can be observed that  $N_{\text{gNB}}^*$  and  $P_t^*$  decrease as  $P_{\text{MD}}$  increases, which in turn improves  $E_C$ . For instance,  $N_{\text{gNB}}^*$  goes from around



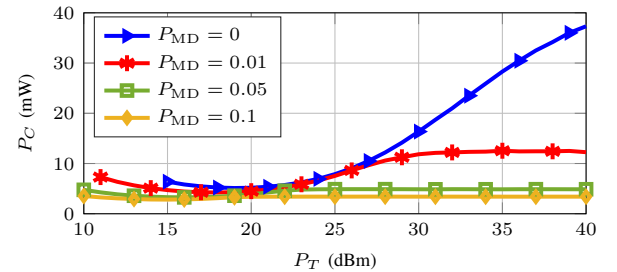
(a) Optimal number of antenna elements  $N_{\text{gNB}}^*$  at the gNB.



(b) Optimal transmission power  $P_t^*$  at the gNB.



(c) Energy consumption  $E_C$ .



(d) Power consumption  $P_C$ .

Fig. 11.  $N_{\text{gNB}}^*$ ,  $P_t^*$ ,  $E_C$ , and  $P_C$  as a function of  $P_T$  and  $P_{\text{MD}}$  for  $v = 1$  m/s,  $T_{SS} = 20$  ms,  $N_{SS} = 8$ ,  $\tau = 7$  dB, and  $K = 200$ . Missing values represent infeasibility.

16.2 to around 2.4 for  $P_T = 18$  dBm as  $P_{\text{MD}}$  increases from 0 to 0.1. This is because a non-zero misdetection probability allows for more UEs to violate the SNR constraint, so the gNB can reduce the number of antennas and the transmission power to save energy, and still make the problem feasible. In addition, as  $N_{\text{gNB}}^*$  decreases, the corresponding beamwidth increases, so the range of feasible values of  $v$  and  $T_{SS}$  to maintain beam alignment increases, which also increases the size of the feasibility regions. For instance,  $P_T \geq 15$  dBm is feasible for  $P_{\text{MD}} = 0$ , while  $P_T \geq 10$  dBm is feasible

TABLE IV  
FEASIBILITY REGIONS FOR  $P_T = 18$  DBM,  $\tau = 7$  DB, AND  $K = 200$ .

$N_{SS} \backslash P_{MD}$		Upper bound on $vT_{SS}$			
		0	0.01	0.05	0.1
8		0.08 m	0.32 m	2.24 m	4.8 m
16		0.16 m	0.64 m	4.8 m	4.8 m
32		0.32 m	1.6 m	4.8 m	4.8 m
64		0.64 m	4.8 m	4.8 m	4.8 m

TABLE V  
FEASIBILITY REGIONS FOR  $P_T = 18$  DBM,  $\tau = 7$  DB, AND  $K = 500$ .

$N_{SS} \backslash P_{MD}$		Upper bound on $vT_{SS}$			
		0	0.01	0.05	0.1
8		0.03 m	0.24 m	2.24 m	4.8 m
16		0.06 m	0.56 m	4.8 m	4.8 m
32		0.14 m	1.28 m	4.8 m	4.8 m
64		0.32 m	4.8 m	4.8 m	4.8 m

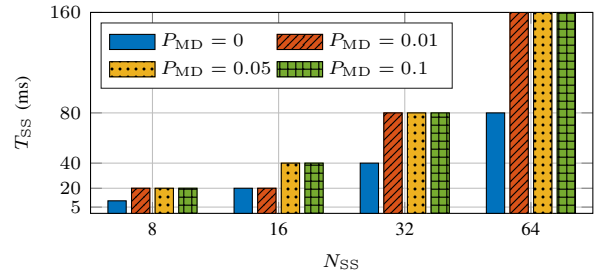
for  $P_{MD} = 0.1$ . Nevertheless,  $N_{gNB}^*$  and  $P_t^*$  eventually saturate when increasing  $P_{MD}$ . In particular,  $N_{gNB}^*$  tends to the minimum feasible value ( $N_{gNB}^* \approx 2$ ), whereas the asymptotic value of  $P_t^*$  decreases as  $P_{MD}$  increases.

Tables IV and V report the upper bound for the feasible product  $vT_{SS}$ , for  $P_{MD}$  ranging from 0 to 0.1 and  $K \in \{200, 500\}$ . According to the results in Sec. V-F, the feasibility region becomes smaller as  $K$  increases for  $P_{MD} = 0$ . Conversely, the impact of  $K$  on the feasibility region becomes negligible when  $P_{MD} > 0$ . On one side, as  $K$  increases there would be more UEs at the cell edge, with an SNR which is close to that of the worst case. On the other side,  $P_{MD} > 0$  would likely mitigate the SNR constraint especially on those worst-case UEs, so that the corresponding feasibility regions would remain unchanged if the two effects are balanced. Fig. 12 depicts the feasibility regions for  $P_T = 18$  dBm,  $\tau = 7$  dB,  $v = 5$  m/s, and  $K \in \{200, 500\}$ , and corroborates these results. We observe that for  $P_{MD} = 0$  and  $N_{SS} = 8$ , the upper bound of the burst periodicity goes from  $T_{SS} = 10$  to 5 ms as  $K$  increases, while for  $P_{MD} > 0$  the limits remain unchanged. A similar behavior can be observed as a function of  $N_{SS}$ .

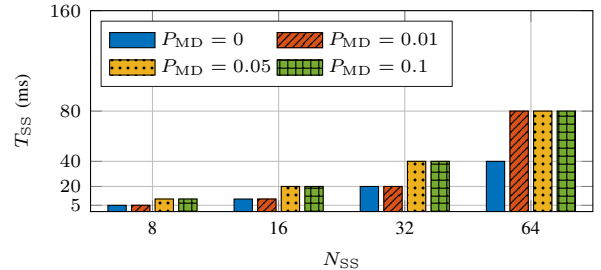
*Summary:* As  $P_{MD} > 0$ , the system is less constrained in terms of SNR, which improves the energy consumption. Also, the size of the feasibility regions tends to increase, so the set of feasible values of  $v$  and  $T_{SS}$  also increases. Finally, the impact of  $K$  is negligible.

#### H. Design Guidelines

The analysis in Sec. V-F suggests that decreasing the duration of beam management, i.e., reducing  $T_{SS}$  and increasing  $N_{SS}$ , promotes feasibility. However, this approach also leads to an increase of the beam management overhead, i.e., more time-frequency resources are used for sending the control signals, and fewer resources are available for data transmission [20]. In fact, even though  $E_C$  is independent of the values of  $v$ ,  $T_{SS}$  and  $N_{SS}$  (see Eq. (4)), and is thus constant within the feasibility region,  $P_C$  is not, as per Eq. (32). Therefore, for a



(a)  $K = 200$ .



(b)  $K = 500$ .

Fig. 12. Feasibility regions for  $P_T = 18$  dBm,  $\tau = 7$  dB,  $v = 5$  m/s, and  $K \in \{200, 500\}$ , considering  $P_{MD} \in \{0, 0.01, 0.05, 0.1\}$ .

TABLE VI  
OPTIMAL REDCAP BEAM MANAGEMENT PARAMETERS FOR  
 $P_T = 18$  DBM AND  $\tau = 7$  DB.

$K \backslash P_{MD}$		Optimal ( $N_{SS}, T_{SS}$ )			
		0	0.01	0.05	0.1
200		8, 10 ms	8, 40 ms	8, 160 ms	8, 160 ms
500		8, 5 ms	8, 40 ms	8, 160 ms	8, 160 ms

given feasible solution  $\{N_{gNB}^*, P_t^*\}$ , we can choose  $T_{SS}$  and  $N_{SS}$  so as to optimize the trade-off between beam management overhead and the resulting energy consumption. In particular, we propose to operate in the top-left part of the feasibility regions, that is choosing the highest feasible  $T_{SS}$  and the lowest feasible  $N_{SS}$ , which therefore represents the optimal beam management configuration for RedCap. This choice still satisfies Constraint  $C_1$  ( $C'_1$ ) of P1 (P2) in terms of SNR since we are within the feasibility regions. Table VI reports the optimal values of  $T_{SS}$  and  $N_{SS}$  for  $P_T = 18$  dBm,  $\tau = 7$  dB,  $v = 5$  m/s,  $K \in \{200, 500\}$ , and  $P_{MD} \in \{0, 0.01, 0.05, 0.1\}$ .

*Summary:* The optimal and feasible beam management configuration for RedCap in terms of both energy efficiency and overhead is to choose the highest possible  $T_{SS}$  and the lowest possible  $N_{SS}$  within the feasibility regions, which in turn determines the corresponding optimal values of  $N_{gNB}^*$  and  $P_t^*$ .

## VI. CONCLUSIONS AND FUTURE WORK

The objective of this work is to minimize the energy consumption of 5G RedCap beam management in an Sma scenario, where both the base station and the end users are battery powered, and thus feature strict energy constraints. To this end, we formalize an optimization problem to choose the number of antenna elements ( $N_{gNB}^*$ ) and the transmission

power ( $P_t^*$ ) at the gNB to minimize energy consumption while guaranteeing a sufficient link quality. Since the problem is an MINLP, we develop a custom algorithm to estimate a feasible solution.

Numerical results show that the optimal number of antennas at the gNB decreases with the maximum transmission power, and increases when considering more demanding SNR constraints. Conversely, the optimal transmission power at the gNB depends on the number of UEs, and is proportional to both the maximum transmission power and the target minimum link quality. Notably, the solution of the optimization problem is independent of the users velocity ( $v$ ) and the beam management parameters, i.e., the SSB burst periodicity ( $T_{SS}$ ) and the number of SSBs per burst ( $N_{SS}$ ). In addition, we identify via simulations, and bound analytically, the feasibility regions of the problem, i.e., the set of parameters for which the optimization problem is feasible. Finally, we observe a trade-off between the energy consumption and the beam management overhead, and propose the optimal feasible beam management configurations for RedCap to optimize the two effects.

As part of our future work, we plan to jointly optimize the energy consumption of both beam management and data transmission, as well as to consider more advanced optimization methods, for example based on machine learning.

#### REFERENCES

- [1] M. Rawat, M. Pagin, M. Giordani, L.-A. Dufrene, Q. Lampin, and M. Zorzi, "Minimizing energy consumption for 5G NR beam management for RedCap devices," in *IEEE GLOBECOM, Kuala Lumpur, Malaysia*, 2023.
- [2] 3GPP, "NR and NG-RAN overall description," TS 38.300, 2018.
- [3] ITU-R, "IMT Vision - Framework and overall objectives of the future development of IMT for 2020 and beyond," Recommendation ITU-R M.2083, Sep. 2015.
- [4] 3GPP, "Service requirements for next generation new services and markets," TS 22.261, 2018.
- [5] L. Atzori, A. Iera, and G. Morabito, "The Internet of Things: A survey," *Comput. Networks*, vol. 54, no. 15, pp. 2787–2805, May 2010.
- [6] A. Zanella, N. Bui, A. Castellani, L. Vangelista, and M. Zorzi, "Internet of Things for Smart Cities," *IEEE Internet Things J.*, vol. 1, no. 1, pp. 22–32, Feb. 2014.
- [7] D. Magrin, M. Centenaro, and L. Vangelista, "Performance evaluation of LoRa networks in a smart city scenario," in *IEEE ICC, Paris, France*, 2017.
- [8] A. P. Matz, J.-A. Fernandez-Prieto, J. Cañada-Bago, and U. Birkel, "A systematic analysis of narrowband IoT quality of service," *Sensors*, vol. 20, no. 6, p. 1636, Mar. 2020.
- [9] G. G. Ribeiro, L. F. de Lima, L. Oliveira, J. J. Rodrigues, C. N. Marins, and G. A. Marcondes, "An outdoor localization system based on SigFox," in *IEEE VTC Spring, Porto, Portugal*, 2018.
- [10] W. Ayoub, A. E. Samhat, F. Nouvel, M. Mroue, and J.-C. Prévotet, "Internet of Mobile Things: Overview of LoRaWAN, DASH7, and NB-IoT in LPWANs standards and supported mobility," *IEEE Commun. Surv. Tutorials*, vol. 21, no. 2, pp. 1561–1581, Secondquarter 2018.
- [11] S. S. H. Hajjaj and K. S. M. Sahari, "Review of agriculture robotics: Practicality and feasibility," in *IEEE IRIS, Tokyo, Japan*, 2016.
- [12] 3GPP, "Study on Communication for Automation in Vertical domains (CAV) – Release 15," TR 22.804, 2020.
- [13] —, "Study on support of reduced capability NR devices - Rel. 17," TR 38.875, 2020.
- [14] N. Varsier, L.-A. Dufrière, M. Dumay, Q. Lampin, and J. Schwoerer, "A 5G New Radio for balanced and mixed IoT use cases: Challenges and key enablers in FR1 band," *IEEE Commun. Mag.*, vol. 59, no. 4, pp. 82–87, May 2021.
- [15] M. Pagin, T. Zugno, M. Giordani, L.-A. Dufrene, Q. Lampin, and M. Zorzi, "5G NR-Light at millimeter waves: Design guidelines for mid-market IoT use cases," *IEEE ICNC, Honolulu, HI, USA*, 2023.
- [16] S.-E. Chiu, N. Ronquillo, and T. Javidi, "Active learning and CSI acquisition for mmWave initial alignment," *IEEE J. Sel. Areas Commun.*, vol. 37, no. 11, pp. 2474–2489, Nov. 2019.
- [17] M. Hussain and N. Michelusi, "Learning and adaptation for millimeter-wave beam tracking and training: A dual timescale variational framework," *IEEE J. Sel. Areas Commun.*, vol. 40, no. 1, pp. 37–53, Jan. 2022.
- [18] M. Scalabrin, N. Michelusi, and M. Rossi, "Beam training and data transmission optimization in millimeter-wave vehicular networks," in *IEEE GLOBECOM, Abu Dhabi, United Arab Emirates*, 2018.
- [19] Y. Wang, M. Narasimha, and R. W. Heath, "MmWave beam prediction with situational awareness: A machine learning approach," in *IEEE SPAWC Wrkshp, Kalamata, Greece*, 2018.
- [20] M. Giordani, M. Polese, A. Roy, D. Castor, and M. Zorzi, "A Tutorial on Beam Management for 3GPP NR at mmWave Frequencies," *IEEE Commun. Surv. Tutorials*, vol. 21, no. 1, pp. 173–196, Firstquarter, 2019.
- [21] M. Giordani and M. Zorzi, "Improved user tracking in 5G millimeter wave mobile networks via refinement operations," in *IEEE Med-Hoc-Net, Budva, Montenegro*, 2017.
- [22] X. Zhao, A. M. A. Abdo, Y. Zhang, S. Geng, and J. Zhang, "Single RF-chain beam training for MU-MIMO energy efficiency and information-centric IoT millimeter wave communications," *IEEE Access*, vol. 7, pp. 6597–6610, Dec. 2018.
- [23] N. Zeulin, A. Ponomarenko-Timofeev, O. Galinina, and S. Andreev, "ML-assisted beam selection via digital twins for time-sensitive industrial IoT," *IEEE Internet Things Mag.*, vol. 5, no. 1, pp. 36–40, Mar. 2022.
- [24] A. Mukherjee, "Energy-efficient beam management in millimeter-wave shared spectrum," *IEEE Wireless Commun.*, vol. 27, no. 5, pp. 38–43, Oct. 2020.
- [25] Ericsson, "RedCap - expanding the 5G device ecosystem for consumers and industries," Ericsson White Paper, 2023.
- [26] A. Traspadini, M. Giordani, G. Giambene, T. De Cola, and M. Zorzi, "On the Energy Consumption of UAV Edge Computing in Non-Terrestrial Networks," in *Asilomar Conference on Signals, Systems, and Computers, Pacific Grove, CA, USA*, 2023.
- [27] 3GPP, "Study on channel model for frequencies from 0.5 to 100 GHz-Release 16," TR 38.901, 2020.
- [28] M. Rawat, M. Giordani, B. Lall, A. Chaoub, and M. Zorzi, "On the Optimal Beamwidth of UAV-Assisted Networks Operating at Millimeter Waves," *IEEE WCNC, Glasgow, United Kingdom*, 2023.
- [29] W. B. Abbas, F. Gomez-Cuba, and M. Zorzi, "Millimeter wave receiver efficiency: A comprehensive comparison of beamforming schemes with low resolution ADCs," *IEEE Trans. Wireless Commun.*, vol. 16, no. 12, pp. 8131–8146, Dec. 2017.
- [30] C. A. Balanis, *Antenna theory: analysis and design*, 4th ed. John Wiley & Sons, Inc, 2015.
- [31] L. N. Ribeiro, S. Schwarz, M. Rupp, and A. L. F. de Almeida, "Energy efficiency of mmWave Massive MIMO precoding with low-resolution DACs," *IEEE J. Sel. Top. Signal Process.*, vol. 12, no. 2, pp. 298–312, Apr. 2018.
- [32] K. Greene, A. Sarkar, and B. Floyd, "A 60-GHz dual-vector Doherty beamformer," *IEEE J. Solid-State Circuits*, vol. 52, no. 5, pp. 1373–1387, May 2017.
- [33] M. Giordani, M. Rebato, A. Zanella, and M. Zorzi, "Coverage and connectivity analysis of millimeter wave vehicular networks," *Ad Hoc Networks*, vol. 80, pp. 158–171, Nov. 2018.
- [34] R. Misener and C. A. Floudas, "ANTIGONE: Algorithms for coNTinuous/Integer Global Optimization of Nonlinear Equations," *J. Global Optim.*, vol. 59, no. 2-3, pp. 503–526, Mar. 2014.
- [35] Gurobi Optimization, LLC, "Gurobi Optimizer Reference Manual," 2023. [Online]. Available: <https://www.gurobi.com>